

## Evidence for dipole nature of the low-energy $\gamma$ enhancement in $^{56}\text{Fe}$

A. C. Larsen,<sup>1,\*</sup> N. Blasi,<sup>2</sup> A. Bracco,<sup>2,3</sup> F. Camera,<sup>2,3</sup> T. K. Eriksen,<sup>1</sup> A. G3rgen,<sup>1</sup>  
M. Guttormsen,<sup>1</sup> T. W. Hagen,<sup>1</sup> S. Leoni,<sup>2,3</sup> B. Million,<sup>2</sup> H. T. Nyhus,<sup>1</sup> T. Renstr3m,<sup>1</sup> S. J. Rose,<sup>1</sup>  
I. E. Ruud,<sup>1</sup> S. Siem,<sup>1</sup> T. Tornyi,<sup>1,4</sup> G. M. Tveten,<sup>1</sup> A. V. Voinov,<sup>5</sup> and M. Wiedeking<sup>6</sup>

<sup>1</sup>*Department of Physics, University of Oslo, N-0316 Oslo, Norway*

<sup>2</sup>*INFN, Sezione di Milano, Milano, Italy*

<sup>3</sup>*Dipartimento di Fisica, University of Milano, Milano, Italy*

<sup>4</sup>*Institute of Nuclear Research, MTA ATOMKI, H-4026 Debrecen, Hungary*

<sup>5</sup>*Department of Physics and Astronomy, Ohio University, Athens, Ohio 45701, USA*

<sup>6</sup>*iThemba LABS, P.O. Box 722, 7129 Somerset West, South Africa*

(Dated: June 24, 2018)

The  $\gamma$ -ray strength function of  $^{56}\text{Fe}$  has been measured from proton- $\gamma$  coincidences for excitation energies up to  $\approx 11$  MeV. The low-energy enhancement in the  $\gamma$ -ray strength function, which was first discovered in the ( $^3\text{He}, \alpha\gamma$ ) $^{56}\text{Fe}$  reaction, is confirmed with the ( $p, p'\gamma$ ) $^{56}\text{Fe}$  experiment reported here. Angular distributions of the  $\gamma$  rays give for the first time evidence that the enhancement is dominated by dipole transitions.

PACS numbers: 25.20.Lj, 24.30.Gd, 27.40.+z

Atomic nuclei are microscopic systems governed by the laws of quantum mechanics. To understand such systems, detailed studies of the accessible quantum-energy levels and their decay properties are vital. The  $\gamma$ -ray strength function ( $\gamma\text{SF}$ ) is a measure of the average, reduced  $\gamma$ -decay probability of the nucleus, and is considered a fruitful concept at high excitation energies where the level spacing is small (the quasi-continuum region).

Structures in the  $\gamma\text{SF}$  provide information on the underlying nuclear dynamics and degrees of freedom, such as the  $M1$  scissors mode [1–3] and the giant electric dipole resonance (GDR) [4]. The  $\gamma\text{SF}$  is also indispensable for predicting reaction cross sections for the astrophysical nucleosynthesis. Specifically, when there is no ( $n, \gamma$ ) – ( $\gamma, n$ ) equilibrium, the shape of the  $\gamma\text{SF}$  in the vicinity of the neutron threshold plays a crucial role for the ( $n, \gamma$ ) reaction rates relevant for the rapid neutron-capture process (r-process) [5, 6].

An enhancement in the  $\gamma\text{SF}$  for  $\gamma$  energies below  $\approx 4$  MeV has been discovered in several  $fp$ -shell and medium-mass nuclei using the Oslo method, such as  $^{56,57}\text{Fe}$  [7] and  $^{93-98}\text{Mo}$  [8]. Recently, the low-energy enhancement (hereby denoted *upbend*) was confirmed in a ( $d, p\gamma$ ) $^{95}\text{Mo}$  experiment [9], using a different detector setup and a model-independent method to extract the  $\gamma\text{SF}$ . The upbend could induce an increase of up to two orders of magnitude in the ( $n, \gamma$ ) reaction rates in very neutron-rich isotopes [10]. Depending on the actual conditions at the astrophysical r-process site, this could be of great importance for the r-process [10].

Despite the potentially crucial role of the upbend for astrophysics applications, its extent and origin remains largely unknown. In particular, the physical mechanism causing the upbend is not understood, mainly because information on the multipolarity and electromagnetic character is lacking. Only for  $^{60}\text{Ni}$  there are data indicating that the upbend is due to  $M1$  transitions [11]. However,  $^{60}\text{Ni}$  might be a special case with only positive-parity states below excitation energies of  $\approx 4.5$  MeV. Up to now, data on Fe isotopes are inconclusive regard-

ing the radiation type; neither  $E1$ ,  $M1$ , or  $E2$  radiation could be excluded (see Fig. 3 in Ref. [7]).

Recent theoretical works on the upbend suggest that it is of  $E1$  nature and due to transitions in the single-(quasi)particle continuum [12], or of  $M1$  type and caused by a reorientation of high- $j$  neutron and proton spins [13]. Apart from the single-particle picture, one could also imagine that strong collective transitions might cause such an enhancement, for example rotational ( $E2$ ) or vibrational ( $E3$ ) transitions in the quasi-continuum.

In this Letter, we show new data on the  $\gamma\text{SF}$  of  $^{56}\text{Fe}$ . The present data set from the inelastic scattering reaction  $^{56}\text{Fe}(p, p'\gamma)^{56}\text{Fe}$  yielded high statistics and allowed for a detailed analysis of the  $\gamma$ -ray angular distributions. We present here for the first time results on the multipolarity of the upbend. To our knowledge, this is also the first time where the angular-distribution analyzing tool has been applied to primary  $\gamma$  transitions with a broad distribution of energies at high excitation energies.

The experiment was performed at the Oslo Cyclotron Laboratory (OCL), using a 16-MeV proton beam with intensity  $\approx 0.5$  nA hitting a self-supporting target of 99.9% enriched  $^{56}\text{Fe}$  with mass thickness of 2 mg/cm<sup>2</sup>. Accumulating time was  $\approx 85$  hours. The charged ejectiles were measured with the Silicon Ring (SiRi) particle-detector system [14] and the  $\gamma$  rays with the CACTUS array [15]. The SiRi system consists of eight  $\Delta E - E$  telescopes, where the front detector is segmented into eight strips ( $\Delta\theta = 2^\circ$ ), covering scattering angles between  $40 - 54^\circ$ . In total, SiRi has a solid-angle coverage of  $\approx 6\%$ . Using the  $\Delta E - E$  technique, each charged-particle species was identified and a gate was set on the outgoing protons. From the reaction kinematics, the proton energy was converted into excitation energy in the residual nucleus.

In this experiment, the CACTUS array contained 22 collimated  $5'' \times 5''$  NaI:Tl detectors, and six collimated  $3.5'' \times 8''$  LaBr<sub>3</sub>:Ce detectors [16, 17]. At the front of the crystals, the conically shaped lead collimators have a radius of 3.5 cm, and

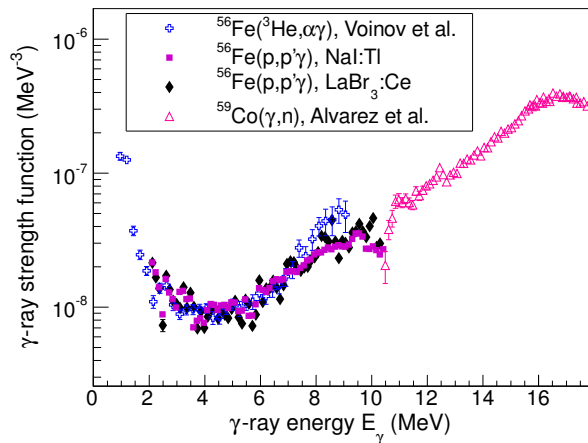


FIG. 1: (Color online) Gamma-strength functions of  $^{56}\text{Fe}$  from the present experiment and from the  $(^3\text{He}, \alpha\gamma)$  data [7] compared with  $^{59}\text{Co}(\gamma, n)$  data from Ref. [26].

the distance to the target is 22 cm, yielding an internal semi-angle of  $9^\circ$ . The NaI detectors were placed in the CACTUS frame with six different angles  $\theta$  with respect to the beam axis: 37.4, 63.4, 79.3, 100.7, 116.6, and 142.6 degrees, while the LaBr<sub>3</sub> crystals covered four angles: 63.4, 79.3, 100.7, and 116.6 degrees.

The  $\gamma$  spectra were unfolded using the technique described in Ref. [18], but with new response functions from  $\gamma$  lines of excited states in  $^{13}\text{C}$ ,  $^{16,17}\text{O}$ ,  $^{28}\text{Si}$ , and  $^{56,57}\text{Fe}$  populated with various inelastic-scattering and transfer reactions. Furthermore, the distribution of the primary  $\gamma$  rays for each excitation-energy bin (124 keV wide) was determined from an iterative subtraction technique [19].

From the matrix of primary  $\gamma$  spectra, we have extracted simultaneously the level density and  $\gamma$ -transmission coefficient for  $^{56}\text{Fe}$  using the least  $\chi^2$  method given in Ref. [20]. The absolute value and slope of the level density were determined from discrete levels [21] below an excitation energy of  $E = 4$  MeV and from the comparison to particle-evaporation data [22, 23]. To get the absolute value of the  $\gamma$ -transmission coefficient, we used estimated values from systematics (as there are no experimental values) for the neutron-resonance level spacing  $D_0 = 2500(1250)$  eV and the total, average  $\gamma$  width  $\langle\Gamma_\gamma\rangle = 1500(750)$  meV, and spin cutoff parameters from Ref. [24]. Assuming that dipole radiation dominates the  $\gamma$  decay in the quasi-continuum region, the  $\gamma$ SF is deduced from the  $\gamma$ -transmission coefficient by

$$f(E_\gamma) = \mathcal{F}(E_\gamma)/2\pi E_\gamma^3, \quad (1)$$

where  $f(E_\gamma)$  is the  $\gamma$ SF for  $\gamma$  energy  $E_\gamma$ , and  $\mathcal{F}(E_\gamma)$  is the  $\gamma$ -transmission coefficient. The resulting  $\gamma$ SFs obtained from the LaBr<sub>3</sub> and NaI  $\gamma$  spectra are shown in Fig. 1.

We observe that our new data are in overall very good agreement with the  $(^3\text{He}, \alpha\gamma)$  data of Ref. [7]. The upbend

is confirmed, using new, higher-resolution detectors and response functions. Also, the different reaction type is expected to populate lower initial spins than the  $(^3\text{He}, \alpha\gamma)$  reaction, which has a high cross section for high- $\ell$  pickup [25]. Compared to the  $(^3\text{He}, \alpha\gamma)$  experiment, the particle-detector resolution has been improved from 400 keV to 90 keV (full-width half maximum), and the  $\gamma$ -energy resolution has been improved by more than a factor of 2 for all  $\gamma$  energies using the LaBr<sub>3</sub> crystals. Thus, the upbend is clearly independent from systematic errors in the detector response and reaction-induced effects. The difference in strength at high  $\gamma$  energies might be due to small variations in the normalization of the level density and the new and more precise response functions. Also, we see a good match with photo-neutron data on  $^{59}\text{Co}$  [26], supporting the chosen values for  $D_0$  and  $\langle\Gamma_\gamma\rangle$ .

Making use of the various angles for which the NaI detectors were placed, angular distributions were extracted by sorting the data into  $(E, E_\gamma)$  matrices according to the angle  $\theta$  of the NaI detectors relative to the beam direction. From the intensities as a function of angle, we have fitted angular-distribution functions of the form [27]

$$W(\theta) = A_0 + A_2P_2(\cos\theta) + A_4P_4(\cos\theta), \quad (2)$$

where  $P_k(\cos\theta)$  is a Legendre polynomial of degree  $k$ . The LaBr<sub>3</sub> detectors were placed at only four angles and were not used for this analysis, although we note that the shape of the angular distributions for the LaBr<sub>3</sub> and NaI detectors are in very good agreement for the four overlapping angles.

The normalized angular-distribution coefficients are given by  $a_k = Q_k \alpha_k A_k / A_0$ , where  $Q_k \approx 1$  is the geometrical attenuation coefficient due to the finite size of the  $\gamma$  detectors, and  $\alpha_k$  is the attenuation due to partial alignment of the nuclei relative to the beam direction. Errors in the intensities are given by  $\sigma_{\text{tot}} = \sigma_{\text{stat}} + \sigma_{\text{sys}}$ , where the statistical errors are estimated with  $\sqrt{N}$  where  $N$  is the number of counts, and the systematic errors are deduced from the relative change in  $N$  for each symmetric pair of angles ( $37.4^\circ, 142.6^\circ$ ), ( $63.4^\circ, 116.6^\circ$ ), and ( $79.3^\circ, 100.7^\circ$ ). Note that for this high-statistics experiment, the statistical error bars are in general small. However, the systematic uncertainties due to partly asymmetric  $\gamma$  intensities for the pairs of angles can in some cases be rather large, which in turn influence the uncertainties in the  $a_k$  coefficients.

The resulting angular distributions for the 4.4-MeV  $E_2$  transition in  $^{12}\text{C}$  and the 6.1-MeV  $E_3$  transition in  $^{16}\text{O}$  are shown in Fig. 2 (a) and (b). Correspondingly, transitions in  $^{56}\text{Fe}$  and  $^{57}\text{Fe}$  are shown in Fig. 2 (c)–(f). The extracted angular-distribution coefficients are given in Tab. I. The stretched dipole, quadrupole and octupole transitions are easily distinguished from each other. We also observe that the attenuation due to partial alignment is becoming less and less pronounced as the excitation energy increases; in fact, the  $a_2^{\text{max}}$  coefficients are in good agreement with the data above  $E \approx 3$  MeV in  $^{56}\text{Fe}$  (see Fig. 2 (e) and (f)).

We now turn to the distribution of primary  $\gamma$  rays as function of excitation energy. The matrix of primary- $\gamma$  spectra

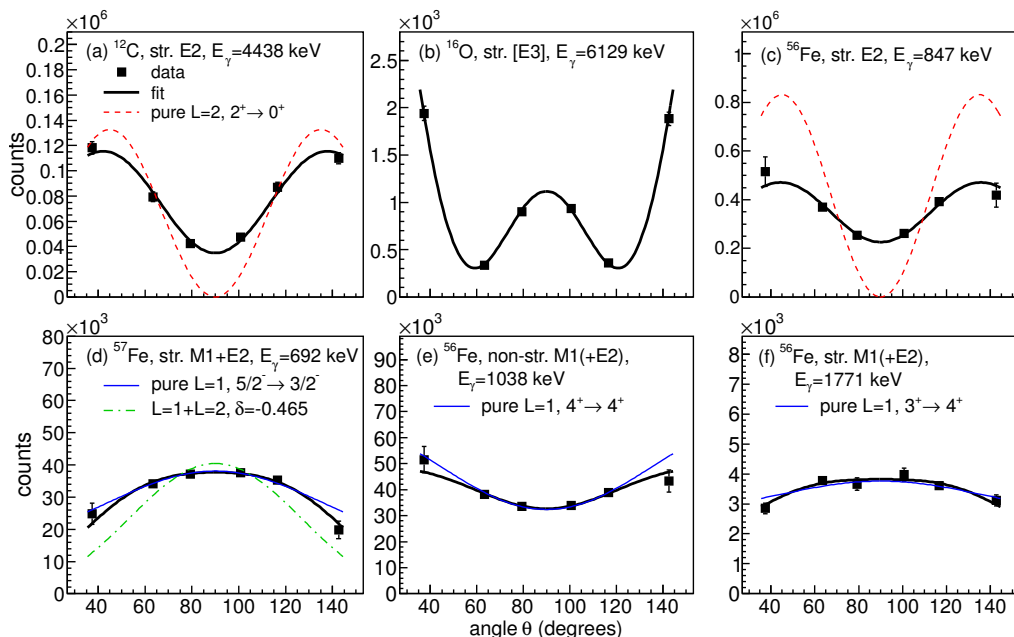


FIG. 2: (Color online) Angular distributions of (a)  $E2$  in  $^{12}\text{C}$ , (b)  $[E3]$  in  $^{16}\text{O}$ , (c)  $E2$  in  $^{56}\text{Fe}$ , (d)  $M1 + E2$  in  $^{57}\text{Fe}$  (mixing ratio  $\delta = -0.465(8)$  [21], giving an  $M1$  fraction of  $\approx 82\%$ ), (e)  $M1(+E2)$  in  $^{56}\text{Fe}$ , and (f)  $M1(+E2)$  in  $^{56}\text{Fe}$ . All data (black squares) are measured with the NaI detectors. The thick, black lines are Legendre fits, the other lines are theoretical distributions [27] with no attenuation (see text).

TABLE I: Angular-distribution coefficients of transitions measured in the present experiment (see text). The theoretical  $a_k^{\max}$  coefficients for complete alignment are taken from Ref. [27].

$^A X$	$E$ (keV)	$E_\gamma$ (keV)	$I_i \rightarrow I_f$	$XL$	$a_2^{\max}$	$a_2$	$a_4^{\max}$	$a_4$
$^{12}\text{C}$	4439	4438	$2^+ \rightarrow 0^+$	$E2$	0.714	0.55(9)	-1.71	-0.77(13)
$^{16}\text{O}$	6130	6129	$3^- \rightarrow 0^+$	$[E3]$	-	1.85(8)	-	1.91(9)
$^{56}\text{Fe}$	847	847	$2^+ \rightarrow 0^+$	$E2$	0.714	0.29(18)	-1.71	-0.60(13)
$^{56}\text{Fe}$	3123	1038	$4^+ \rightarrow 4^+$	$M1(+E2)$	0.500	0.31(13)	0.00	-0.09(8)
$^{56}\text{Fe}$	3856	1771	$3^+ \rightarrow 4^+$	$M1(+E2)$	-0.167	-0.33(8)	0.00	-0.11(14)
$^{56}\text{Fe}$	4510	3663	$3^- \rightarrow 2^+$	$(E1)$	-0.400	-0.31(16)	0.00	0.07(13)
$^{56}\text{Fe}$	5122	3037	$5^- \rightarrow 4^+$	$(E1)$	-0.333	-0.42(15)	0.00	0.20(17)
$^{57}\text{Fe}$	706	692	$5/2^- \rightarrow 3/2^-$	$M1 + E2$	-1.068	-0.69(12)	0.12	-0.18(9)

for  $^{56}\text{Fe}$  is displayed in Fig. 3. For  $\gamma$  decay in the quasi-continuum below the neutron threshold, the  $\gamma\text{SF}$  is dominated by the tail of the GDR. In addition, the Giant Magnetic Dipole Resonance (GMDR), has its maximum at typically  $E_\gamma = 8$  MeV [28]. Thus, the region of high excitation energy (above  $\approx 5 - 6$  MeV) is expected to be dominated by dipole transitions.

In the present experiment, the reaction populates a range of initial spins in the quasi-continuum. From the primary transitions we can clearly identify initial spins up to 6. The angular distributions represent a mix of stretched and non-stretched dipole transitions; if an initial level with spin 4 is populated, it might de-excite with a dipole transition to a final level with spin 3, 4, or 5. Two of these transitions are stretched and one is non-stretched, therefore, one expects that on average 2/3 of

the transitions are stretched and 1/3 are non-stretched.

The angular distributions for a non-stretched and a stretched  $M1(+E2)$  transition in  $^{56}\text{Fe}$  are shown in Fig. 2 (e) and (f), while in Fig. 4 (a) a stretched ( $E1$ ) transition is displayed. The angular distribution of high-energy  $\gamma$  rays for  $E > 6.6$  MeV is shown in Fig. 4 (b), and for a narrow gate in the region of the upbend in Fig. 4 (c), with a shape consistent with a stretched dipole (the exact initial and final spin is unknown). A theoretical distribution assuming a  $4 \rightarrow 3$  transition is shown, using values of  $a_2^{\max} = -0.357$ ,  $a_4^{\max} = 0.0$  [27], to be compared with the values from the fit,  $a_2 = -0.35(4)$ ,  $a_4 = -0.10(6)$ . The angular distribution for the whole low-energy region (the box in Fig. 3) is displayed in Fig. 4 (d), clearly resembling the high-energy part.

To determine the angular-distribution coefficients for the

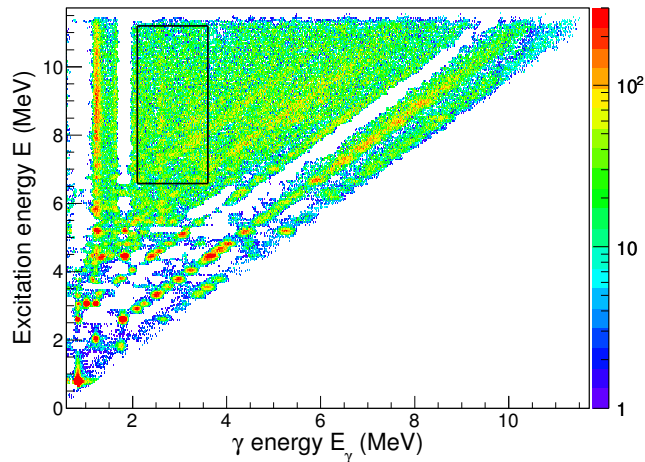


FIG. 3: (Color online) Distribution of primary  $\gamma$  rays in  $^{56}\text{Fe}$  from the NaI detectors at  $79.3^\circ$ . The box indicates the region used for the angular distributions of  $E_\gamma < 3.6$  MeV.

high-energy  $\gamma$  rays and in the region of the upbend, we have performed independent fits of Eq. (2) to 720-keV wide excitation-energy slices of the primary  $\gamma$  matrix. Then, a linear fit was performed for all the extracted angular-distribution coefficients, giving  $a_2 = -0.07(1)$ ,  $a_4 = -0.09(1)$  and  $a_2 = -0.12(3)$ ,  $a_4 = -0.08(3)$  for the low and high-energy  $\gamma$  rays, respectively (dashed lines in Fig. 4). The  $a_k$  coefficients for the two energy regions are compatible within  $1\sigma$ , which indicate that the nature of these  $\gamma$  rays is very similar. By applying a weight of  $2/3$  for the stretched and  $1/3$  for the non-stretched known dipole transitions in  $^{56}\text{Fe}$  as given in Tab. I ( $E_\gamma = 1038, 1771, 3037$  and  $3663$  keV), the expected  $a_k$  coefficients for the quasi-continuum decay are  $a_2 = -0.13(7)$  and  $a_4 = -0.01(5)$ , further supporting that both the low and high-energy  $\gamma$  regions are dominated by dipole transitions. Based on these findings, we can exclude that the upbend is due to stretched quadrupole ( $E2$ ) or octupole ( $E3$ ) transitions.

We have also considered expected distributions with  $a_k^{\text{max}}$  coefficients [27] for an initial spin range  $I_i = 1 - 6$  and final spins  $I_f = 0 - 7$  for stretched and non-stretched dipole transitions, yielding the distribution shown as a blue line in Fig. 4 (b) and (d). If we assume that there are only quadrupole transitions (stretched and non-stretched,  $I_f = 0 - 8$ ), the fit is much worse and the data are clearly not reproduced (red lines in Fig. 4 (b) and (d)). The best reproduction of the experimental angular distributions was found with a 90% and 10% weight on the dipole and stretched-quadrupole contribution ( $6 \rightarrow 4, 5 \rightarrow 3, 4 \rightarrow 2, 3 \rightarrow 1$ ). For an increased weight on the quadrupole contribution, or taking non-stretched and  $4 \rightarrow 6, \dots$  quadrupoles into account, the fit was significantly worse. Therefore, we conclude that  $E2$  transitions are of minor importance and that dipole transitions dominate both the region of the upbend and for the high-energy  $\gamma$ s. Our findings

support the  $L = 1$  assumption applied in Eq. (1).

To summarize, we have presented in this Letter a new measurement on the  $\gamma$ -strength function of  $^{56}\text{Fe}$ . The upbend in the strength, which may have profound consequences for r-process reaction rates, is confirmed with an improved detector setup and response functions, and with a different reaction and beam energy. We have demonstrated that the angular distribution of the low-energy primary  $\gamma$  rays is consistent with a mixture of stretched and non-stretched dipole transitions, and that quadrupole and octupole transitions are of minor importance. Thus, for the first time, the multipolarity of the upbend has been measured and shown to exhibit predominantly a dipole character.

A. C. L. gratefully acknowledges funding of this research from the Research Council of Norway, project grant no. 205528. M. W. acknowledges support from the National Research Foundation of South Africa. We would like to give special thanks to E. A. Olsen, J. C. Müller, A. Semchenkov, and J. C. Wikne for providing the high-quality beam and excellent experimental conditions.

\* Electronic address: a.c.larsen@fys.uio.no

- [1] K. Heyde *et al.*, *Rev. Mod. Phys.* **82**, 2365 (2010).
- [2] A. Schiller *et al.*, *Phys. Lett. B* **633**, 225 (2006).
- [3] M. Krtička *et al.*, *Phys. Rev. Lett.* **92**, 172501 (2004).
- [4] M. N. Harakeh and A. van der Woude, *Giant Resonances*, Oxford University Press (2001).
- [5] S. Goriely, *Phys. Lett.* **B436**, 10 (1998).
- [6] M. Arnould *et al.*, *Phys. Rep.* **450**, 97 (2007).
- [7] A. Voinov *et al.*, *Phys. Rev. Lett.* **93**, 142504 (2004).
- [8] M. Guttormsen *et al.*, *Phys. Rev. C* **71**, 044307 (2005).
- [9] M. Wiedeking *et al.*, *Phys. Rev. Lett.* **108**, 162503 (2012).
- [10] A. C. Larsen and S. Goriely, *Phys. Rev. C* **82**, 014318 (2010).
- [11] A. V. Voinov *et al.*, *Phys. Rev. C* **81**, 024319 (2010).
- [12] E. Litvinova *et al.*, *Phys. Rev. C* **88**, 031302(R) (2013).
- [13] R. Schwengner *et al.*, submitted to *Phys. Rev. Letters* (2013).
- [14] M. Guttormsen *et al.*, *Nucl. Instrum. Methods Phys. Res. A* **648**, 168 (2011).
- [15] M. Guttormsen *et al.*, *Phys. Scr.* **T 32**, 54 (1990).
- [16] A. Giaz *et al.*, *Nucl. Instrum. Methods Phys. Res. A* **729**, 910 (2013).
- [17] R. Nicolini *et al.*, *Nucl. Instrum. Methods Phys. Res. A* **582**, 554 (2007).
- [18] M. Guttormsen *et al.*, *Nucl. Instrum. Methods Phys. Res. A* **374**, 371 (1996).
- [19] M. Guttormsen, T. Ramsøy, and J. Rekestad, *Nucl. Instrum. Methods Phys. Res. A* **255**, 518 (1987).
- [20] A. Schiller *et al.*, *Nucl. Instrum. Methods Phys. Res. A* **447** 498 (2000).
- [21] Data extracted using the NNDC On-Line Data Service from the ENSDF database, August 2013; <http://www.nndc.bnl.gov/ensdf/>.
- [22] A. V. Voinov *et al.*, *Phys. Rev. C* **74**, 014314 (2006).
- [23] H. K. Vonach and J. R. Huizenga, *Phys. Rev.* **149**, 844(1966).
- [24] T. von Egidy and D. Bucurescu, *Phys. Rev. C* **80**, 054310 (2009).
- [25] R. F. Casten *et al.*, *Mat. Fys. Medd. Dan. Vid. Selsk.* **38**, no. 13 (1972).

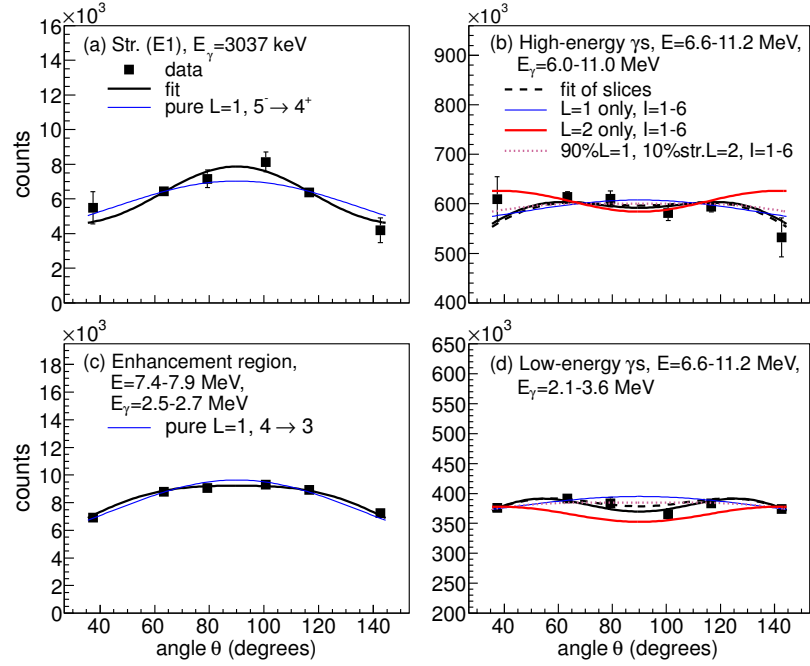


FIG. 4: (Color online) Angular distributions from the primary- $\gamma$  matrix of  $^{56}\text{Fe}$ : (a) ( $E1$ ) transition; (b) high-energy primary  $\gamma$  rays; (c) narrow  $E, E_\gamma$  gate in the low-energy  $\gamma$  region; (d) low-energy primary  $\gamma$  rays. The thick, black lines show the fit to the data, and the thin blue line gives theoretical dipole distributions. For (b) and (d) the dashed lines show the angular distributions from the fit of many  $E$  slices, the blue (red) lines give the theoretical curves for dipole (quadrupole) transitions from initial spins  $I_i = 1 - 6$ , and the pink, dotted lines are theoretical curves for a mix of  $L = 1$  and  $L = 2$  transitions (see text). Note the different scale on the y axis for (b) and (d).

[26] R. A. Alvarez *et al.*, Phys. Rev. C **20**, 128 (1979).

[27] E. der Mateosian and A. W. Sunyar, At. Data and Nucl. Data Tables **13**, 391 (1974).

[28] R. Capote *et al.*, Reference Input Parameter Library, Nucl. Data Sheets **110**, 3107 (2009).